



High-performance ZIF-8/biopolymer chitosan mixed-matrix pervaporation membrane for methanol/dimethyl carbonate separation

Xiao Xu^{a,b,*}, Yusak Hartanto^{a,b}, Daria Nikolaeva^{a,b}, Zirui He^{a,b}, Sara Chergaoui^{a,b}, Patricia Luis^{a,b,*}

^a Institute of Mechanics, Materials and Civil Engineering - Materials & Process Engineering (IMMC-IMAP), UCLouvain, Place Sainte Barbe 2, 1348 Louvain-la-Neuve, Belgium

^b Research & Innovation Centre for Process Engineering (ReCIPE), Place Sainte Barbe, 2 bte L5.02.02, B-1348 Louvain-la-Neuve, Belgium

ARTICLE INFO

Keywords:

Methanol/dimethyl carbonate separation
Mixed matrix membranes
Biopolymer chitosan
Metal-organic frameworks
Pervaporation

ABSTRACT

The separation of dimethyl carbonate (DMC) –an ecofriendly organic compound– from a reaction medium is oftentimes complicated due to the presence of other organic compounds, particularly when the mixture forms an azeotrope. To this end, pervaporation is proposed in this work as the perfect candidate to solve this separation puzzle, using novel membranes which flipped the ratio of the binary mixture methanol (MeOH) and DMC (from 10:90 to ~90:10). ZIF-8 fillers were incorporated into chitosan (CS) biopolymer matrix to prepare these mixed-matrix membranes (MMM). At 15 wt% loading of ZIF-8/CS, the ~30 μm-thick MMM showed an exceptional selectivity of 11.2, with MeOH permeance of 97.7 GPU at 50 °C. This superior separation performance is attributed to the higher MeOH affinity to the CS matrix, further reinforced with the preferential channels of ZIF-8 fillers for MeOH. This successful separation of binary organic mixtures elevates a crucial part of downstream processing, merely achieved with conventional distillation, and most importantly, open doors to greener fuels.

1. Introduction

Dimethyl carbonate (DMC) has been considered an environmentally friendly organic compound due to its biodegradability and low toxicity [1]. In recent years, extensive research on DMC as an effective biofuel and diesel fuel additive has been performed [2–6]. This oxygenated compound can reduce the energy density of fuel mixtures due to its low calorific value, thereby reaching a high level of fossil fuel substitution [7]. This compound also paves the way to synthesize less toxic products that can substitute methyl halides, dimethyl sulfate and phosgene in the chemical and pharmaceutical industries [8]. A case in point is the valorization of crude glycerol, a by-product of biodiesel production using biomass materials such as vegetable oils, animal fats, waste cooking oils and fats [9–13]. In this bio-based transesterification reaction, glycerol carbonate is formed during this process besides MeOH [15]. Besides, an excess of DMC is required for acquiring a higher yields of glycerol carbonate. However, the separation of MeOH from the products' mixture consumes significant energy since MeOH and DMC reach an azeotrope at a methanol concentration of 85 mol% at atmospheric pressure [14]. In this context, an effective separation of MeOH/

DMC is essential. A variety of separation processes e.g., extractive distillation [15] and pervaporation [16], or the utilization of ionic liquids as entrainers [17], have been proposed to separate MeOH/DMC. However, the energy consumption has been a critical hurdle in those techniques, hence other separation approaches must be investigated.

Pervaporation (PV) consumes less energy and is cost-effective [16,18], attracting the attention of membranologists to investigate the separation of azeotropic mixtures, the recovery of heat sensitive compounds and removal of low concentrated pollutants from aqueous solutions [19–21]. The range of PV applications is very broad, including: (1) organic dehydration; (2) solvent recovery or removal from wastewater; (3) separation of organic mixtures. The latter is the most challenging, as the components of these mixtures in most cases, have very similar physical and chemical properties, making this type of separation needs to be dealt with on a case-by-case basis [14].

Polymeric membranes have advantages of good processability, low cost and ease of production scale-up [22]. Several synthetic polymers are typically used to prepare PV membranes, such as polyvinyl alcohol (PVA), PEBA, polydimethylsiloxane (PDMS), and polyimide (PI) [22]. Biopolymers, such as chitosan (CS) provided from biomass waste, have

* Corresponding authors.

E-mail addresses: xiao.xu@uclouvain.be (X. Xu), patricia.luis@uclouvain.be (P. Luis).

<https://doi.org/10.1016/j.seppur.2022.121085>

Received 11 January 2022; Received in revised form 13 April 2022; Accepted 13 April 2022

Available online 22 April 2022

1383-5866/© 2022 Elsevier B.V. All rights reserved.

also been used to prepare PV membranes due to its unique properties, such as biodegradability, biocompatibility, and non-toxicity [23,24]. However, CS-based membranes have also been facing the permeability/selectivity trade-off limitation [20]. Various inorganic fillers are incorporated in CS-based membranes to overcome this constraint, such as carbon molecular sieves, zeolites, and carbon nanotubes [25–28]. Nevertheless, the interface incompatibility between inorganic fillers and the polymer matrix often plagues the process of the producing mixed matrix membranes (MMMs) and thus further modifications are needed to reduce or eliminate non-selective volumes at the interface between inorganic fillers and polymers [29,30]. Instead, organic fillers like metal organic frameworks (MOFs), are a better alternative showing better compatibility than inorganic ones [31].

MOFs, a combination of metal ions and organic ligands, are organic materials that generally have 3-D nanostructures, large specific surface areas and adjustable adsorption capacity [32,33]. Because of these properties, MOFs have attracted significant attention for MMMs. Zeolitic imidazolate frameworks (ZIFs), formed by connecting tetrahedral metal ions (e.g., Zn, Co) through imidazolate anions, are a subclass of MOFs which have similar structures to zeolites [34]. ZIFs have been utilized as the fillers for MMMs in PV. For example, Amirilargani *et al.*, [35] distributed ZIF-8 particles into polyvinyl alcohol for isopropanol dehydration using PV. The total flux increased in contrast with pure polymeric membrane, but with the expense of the separation factor. Likewise, nanoscale ZIF-90 crystals were also embedded into P84 polymeric membranes for the dehydration of isopropanol solution, and the flux increased without compromising the separation factor at the adequate loading of ZIF-90 [36]. In addition, ZIFs have also been used for PV recovery of organics. Liu *et al.*, [37] used ZIF-71/ polyether-block-amide MMMs to recover biobutanol from acetone-butanol-ethanol fermentation broth. Kang *et al.* [38] distributed ZIF-7 particles into CS matrix for the production of ZIF-7/CS MMMs to extract ethanol from an aqueous solution. The abovementioned membranes broke through the permeability/selectivity trade-off, but there are limited studies regarding the preparation of ZIFs/CS MMMs for the pervaporation dehydration and recovery applications [20,38], and there is no study of ZIFs/CS MMMs for the separation of organic-organic mixtures in PV.

The synthesis of a ZIFs/CS MMMs and their performance in separating of organic-organic mixture is studied in this work, which is first in the literature. ZIF-8 is a highly suitable molecular sieve for the extraction of MeOH from MeOH/DMC. Owing to the flexibility of ZIF-8, the effective window size of ZIF-8 is 0.40–0.42 nm, while the kinetic diameter of MeOH and DMC are 0.38 nm and 0.47–0.63 nm, respectively [39,40]. Furthermore, there is abundance of $-OH$ and $-NH_2$ on the surface of ZIF-8. These groups can form hydrogen bonds with the $-OH$ or $-NH_2$ of CS, thereby promoting the compatibility between the ZIF-8 particles and CS [41] and leading to more effective membranes. In the present study, small-size ZIF-8 particles were first synthesized and characterized. They were then incorporated into CS to fabricate free-standing ZIF-8/CS MMMs. Finally, the fabricated MMMs were characterized and their separation performance of MeOH/DMC using PV was evaluated.

2. Experimental section

2.1. Materials

Zinc nitrate hexahydrate ($Zn(NO_3)_2 \cdot 6H_2O$, 99%), 2-Methylimidazole (Hmim, 97%) and Dimethyl carbonate (DMC, 99%) were purchased from Alfa Aesar (Germany). The CS polymer powder (low molecular weight) was obtained from Sigma-Aldrich (US). Absolute ethanol (C_2H_5OH , 99.9%), ethanalamine ($NH_2CH_2CH_2OH$, 99.5%), triethylamine (TEA, $N(CH_2CH_3)_3$, 99.5%), methanol (MeOH, 100.0%) and acetic acid (CH_3COOH , 99.8%) were provided by VWR International (Belgium). All chemicals were used as received.

2.2. Synthesis of ZIF-8 particles

Submicron-sized ZIF-8 particles were synthesized according to the aqueous room-temperature method listed in [42]. First, 2 g of $Zn(NO_3)_2 \cdot 6H_2O$ was dissolved in 12.11 g of deionized water to prepare $Zn(NO_3)_2$ solution. Besides, 3.312 g of Hmim was dissolved in 48.45 g of deionized water to prepare Hmim solution. Then, 3.0 ml of TEA was added into Hmim solution. Subsequently, these two solutions were mixed for 0.5 h. The product was centrifuged at 4000 rpm for 15 min and subsequently washed with deionized water twice and with absolute ethanol once. The obtained product was dried under vacuum oven at 120 °C for 10 h.

2.3. Membrane preparation

MMMs were synthesized with 1.0 g of CS powders dissolved in 49.0 g of 2 wt% CH_3COOH solution and stirred at room temperature for 2 h. A certain quantity of ethanalamine was then added to adjust the pH of the solution to ≥ 4 because ZIF-8 can maintain the good crystallinity after being immersed in aqueous solution of pH = 4 for 3 days [43]. The solution was stirred for another 24 h until chitosan and ethanalamine formed a homogenous solution. The required amounts of ZIF-8 particles were dispersed into chitosan solution and stirred for 12 h to allow for an even distribution of ZIF-8 particles into CS solution. The membranes were prepared using solvent evaporation method. Briefly, a certain amount of the dope solution was poured onto clear cellophane with a retainer ring made of stainless steel and dried in a fume hood for 2 days. The membranes after solvent evaporation were peeled off gently. The membranes thickness was measured using the Mitutoyo micrometer and the thickness is 36–43 μm . The loading of ZIF-8 in MMMs was defined as.

$$\omega_{ZIF-8} = \frac{m_{ZIF-8}}{m_{ZIF-8} + m_{CS}} \times 100\% \quad (1)$$

wherein ω_{ZIF-8} is the ZIF-8 particle loading, m_{ZIF-8} and m_{CS} represent the masses of ZIF-8 and CS, respectively.

The ZIF-8 particle loadings in the present study were varied as 0, 0.05, 0.1, 0.15, 0.20 and 0.25 and the resulting membranes were designated as M-0, M-5, M-10, M-15, M-20 and M-25, respectively.

2.4. Membrane characterization

Scanning Electron Microscope (SEM) (Zeiss, ULTRA with Bruker EDS chemical analyzer) was employed to portray the morphology of the fabricated membranes. Membranes were beforehand immersed into liquid nitrogen for a clean cross-sectional cut. Next, a thin layer of gold was deposited under vacuum with a sputter coater (BALZERS UNION FL 9460 BALZERS SCD 030) to make the samples conductive. As for the crystallinity of ZIF-8 particles and membranes, it was investigated using X-ray diffraction (XRD, Bruker D8 Advance, Cu $K\alpha$ radiation, $\lambda = 1.5406 \text{ \AA}$) in the range from 6 to 60°, while FT-IR spectra of ZIF-8 and membranes were obtained using Bruker spectrometer from 400 cm^{-1} to 4000 cm^{-1} in ATR mode to investigate the chemical property of all the membrane samples. Finally, the thermal gravimetric analyses (TGA) were carried out on dried samples of ZIF-8 and membranes. It was used to verify whether the chemical change of the membrane causes changes in the way the material loses water and degrade during heating. DYN-THERM TGA was used with a 15 °C/min heating rate from 25 °C to 800 °C under 300 Nml/min Ar sweep gas flow at atmospheric pressure.

2.5. Solvent uptake

Solvent uptake tests on the membranes were carried out gravimetrically using an analytical balance (Mettler AE 260 DeltaRange). Before conducting solvent uptake, membranes with different loadings were dried in a vacuum oven at 100 °C for 24 h to remove residual solvents. Afterwards, the dried membrane samples were immersed in pure MeOH,

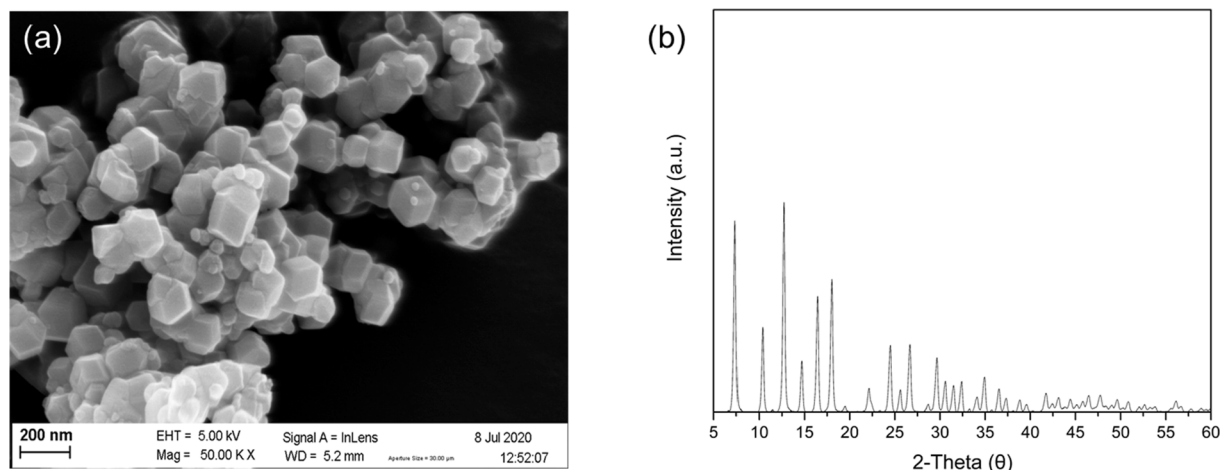


Fig. 1. (a) SEM image of ZIF-8 particles and (b) XRD pattern of the as-synthesized ZIF-8 particles.

DMC and feed solution with the MeOH/DMC molar ratio of 10:90, respectively, in sealed bottles at 50 °C. The swollen membrane samples (W_1) were weighed as quickly as possible after wiping off all solvents on the membrane surface with tissue papers at specific time intervals. This process was continued until no weight changes were observed. After weighing, the membrane samples were re-dried at 100 °C for 24 h in a vacuum oven to evaporate all of the adsorbed solvent. The re-dried membrane samples were weighted again (W_2). All the experiments were performed at least three times. The solvent uptake ratios were determined by the following equations [44,45]:

$$\text{Solvent uptake ratios \%} = \frac{W_1 - W_2}{W_2} \times 100\% \quad (2)$$

The solvent uptake is correlated with the Hansen solubility parameters (HSP), which have been employed to evaluate the compatibility between the filler and the polymer matrix as well as the affinity of materials to solvents [46,47]. The compatibility among MeOH, DMC, ZIF-8 and polymer can be evaluated by the equation (3):

$$\delta^2 = (\delta_d^2 + \delta_p^2 + \delta_h^2)^{1/2} \quad (3)$$

where δ_d , δ_p and δ_h with the subscripts d , p and h , represent the vectors for dispersion, polar and hydrogen bonding contributions, respectively, in three-dimensions known as the Hansen space. δ is the total solubility, corresponding to one point in the Hansen space. The distance between point 1 (e.g., the polymer) and point 2 (e.g., the solvent) is expressed by the following equation:

$$R_a = [4(\delta_{d1} - \delta_{d2})^2 + (\delta_{p1} - \delta_{p2})^2 + (\delta_{h1} - \delta_{h2})^2]^{1/2} \quad (4)$$

where R_a is the solubility distance parameter between two components. The smaller the R_a , the higher the affinity [47].

The Hansen solubility parameters of mixture can be determined by following equation [48]:

$$\bar{\delta} = \sum_i \phi_i \delta_{ki} \quad (5)$$

In which the subscript ki indicates the d , p and h corresponding to component i , and ϕ_i is the volume fraction of component i in the mixture.

2.6. PV experiments

All PV experiments were conducted in a 3-inch round cell module (Sulzer Chemtech GmbH, Switzerland) with an effective membrane surface area of 38.48 cm² (diameter 7.0 cm) [49,50]. Unless otherwise

stated, a MeOH/DMC mixture of 10/90 (mol%) was used as the feed solution. The feed solution was circulated in the setup for 2 h to reach steady state conditions before beginning the permeate sample collection. The pressure on the permeate side was maintained below 2 mbar using a vacuum pump. The permeate were collected using a cold trap at regular intervals and weighed using an analytical balance. The compositions of the feed and permeate samples were analyzed by gas chromatography (Thermo Scientific™ - TRACE 1300 Gas Chromatograph) equipped with a flame ionization detector (FID). The change of the feed concentration can be neglected during the evaluation due to the large amount of the feed solution (at least 1 L), in contrast with the permeate samples. In addition, each experiment was carried out at least three times to ensure the reliability and the repeatability of the results.

The performance of the membranes in pervaporation can be determined by four parameters, namely, transmembrane flux J (g/m²·h), separation factor $\beta_{i/j}$, permeance P_i/l and selectivity $\alpha_{i/j}$, defined as follows:

$$J = \frac{Q}{\Delta t \times A} \quad (6)$$

$$\beta_{i/j} = \frac{y_i/y_j}{x_i/x_j} \quad (7)$$

$$P_i/l = \frac{J_i}{(x_i \times \gamma_i \times P_i^0 - y_i \times P_p)} \quad (8)$$

$$\alpha_{i/j} = \frac{P_i/l}{P_j/l} = \frac{P_i}{P_j} \quad (9)$$

where Q represents the weight of the collected permeate sample (g), A is the effective membrane area (m²) and Δt is the time interval during the sample collection (h); x and y are the molar fractions in the feed and permeate, respectively; the subscripts i and j indicate the components MeOH and DMC, respectively; J_i is the permeation flux of component i (g/m²·h), γ_i is the activity coefficient of component i in the feed, and P_i^0 is the saturated vapor pressure of pure component i , while P_p is the total pressure at the permeate side. P_i is the permeability of component i and l represents the membrane thickness. Non-random two-liquid method (NRTL) used to calculate γ_i of MeOH and DMC in the binary mixture at different temperatures and different concentrations. The specific equations of γ_i have been included as Supporting information (Figs. S.1-S.5). The liquid permeance is also often expressed in gas permeation units (GPU) [51], such that:

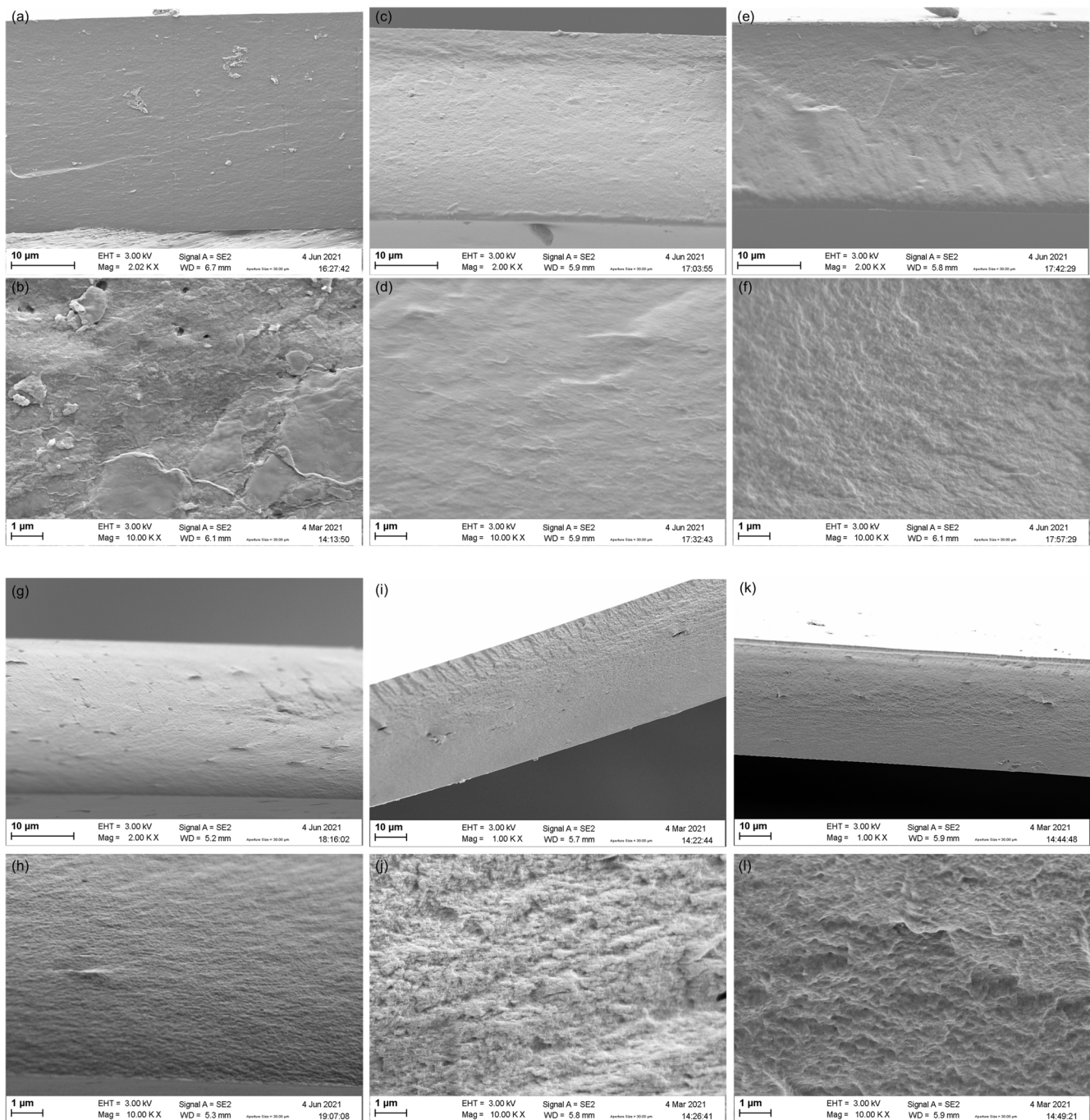


Fig. 2. SEM images at different loadings of MMMs (a-b: 0 wt%, c-d: 5 wt%, e-f: 10 wt%, g-h: 15 wt%, i-j: 20 wt%, k-l: 25 wt% loading).

$$1\text{GPU} = 1$$

$$\times 10^{-6} \text{cm}^3(\text{STP}) / (\text{cm}^2 \text{scmHg}) \text{ and } 1\text{m}^3 / (\text{m}^2 \text{skPa}) = 1.33 \times 10^8 \text{GPU}$$

3. Results and discussion

3.1. Characterization of ZIF-8

Fig. 1a shows the SEM images of the as-fabricated ZIF-8 particles. The size of the as-synthesized ZIF-8 particles was in the range of 100–200 nm. This small size is critical because common blending method cannot effectively separate intergrown ZIF-8 crystals into individual crystals, so the generation of submicron-sized crystals can facilitate the preparation of membranes around several tens of microns thick

[52].

Furthermore, the reduced-sized crystals as the fillers within polymer matrix can reduce non-selective volumes in the filler/polymer interface and thus high membrane selectivity can be achieved [52]. The XRD analysis showed a crystalline structure of ZIF-8 with characteristic peaks at 2θ values of 7° , 10° , 12° , 14° , 18° , 22° , 24° , 26° , 29° , 33° , 34° and 35° , as shown Fig. 1b. The XRD pattern of as-synthesized ZIF-8 are consistent with those in literature [42,53], indicating that highly-crystalline ZIF-8 without other impurities was obtained in this study.

3.2. Membrane characterization

3.2.1. Morphology of the membranes and mechanical properties

The cross sections of the prepared MMMs with different ZIF-8

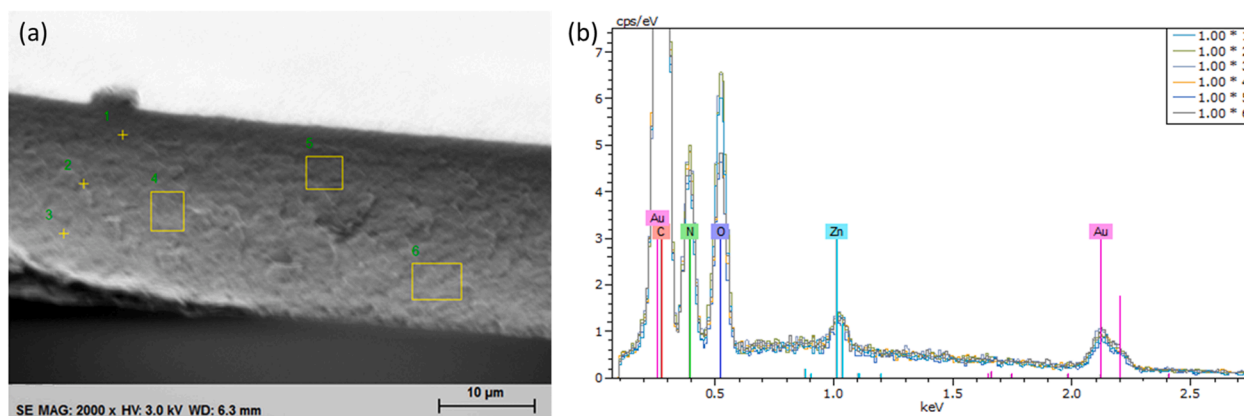


Fig. 3. SEM images (a) and EDX analysis (b) of 15 wt% ZIF-8 loaded MMM.

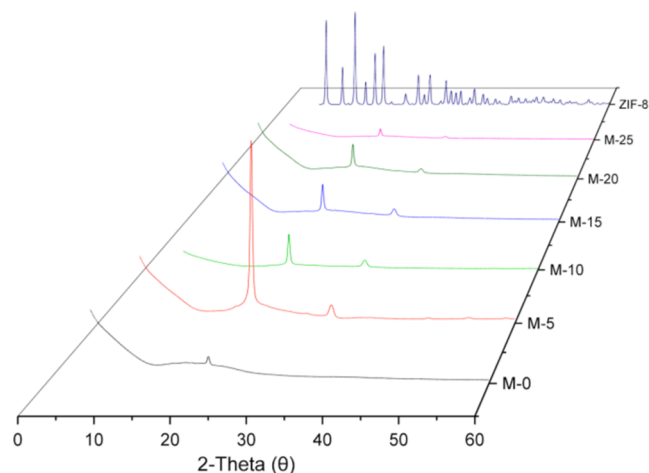


Fig. 4. XRD patterns of ZIF-8 powders and ZIF-8/CS MMMs with different particle loadings.

loadings were characterized by SEM. As observed from Fig. 2 (a) and (b), the pristine CS membrane had a smooth and dense cross section but there exist some defects. The images in Fig. 2 (c) – (l) show that ZIF-8 particles were well-distributed in CS matrix, with no apparent holes or cracks, indicating a good interfacial compatibility between ZIF-8 crystals and the polymer matrix. However, as the amount of incorporated ZIF-8 increased, the cross-section of MMMs turned rougher, with a less dense membrane structure, which can be attributed to the disruption of CS polymer chain packing by the presence of ZIF-8 particles.

The energy dispersive spectrometer (EDS) pattern of the 15 wt% ZIF-8 loaded MMM (Fig. 3) shows that the main element of ZIF-8 i.e., Zn, appeared on 6 different areas of the membrane (including 3 points and 3 rectangle boxes) and the intensity of all the Zn peaks in the EDS spectrum is the same. This indicates that ZIF-8 particles are distributed uniformly within the membrane.

In addition, mechanical properties of pure chitosan membrane and 15 wt% ZIF-8 loaded MMM were measured by nanoindentation [54]. It can be observed that the loading curves do not overlap with the unloading curves, suggesting that the membranes are not totally elastic though they show plastic behaviour [55]. Compared to the pure chitosan membrane, the 15 wt% ZIF-8 loaded MMM showed both higher hardness and elastic modulus (Fig. S6). As anticipated, the incorporation of ZIF-8 particles into chitosan matrix has a dramatic effect on hardness and resistance to elastic deformation as the stress is applied [56].

3.2.2. The crystalline form of the developed MMMs

XRD spectrum for membranes with different ZIF-8 loadings (Fig. 4)

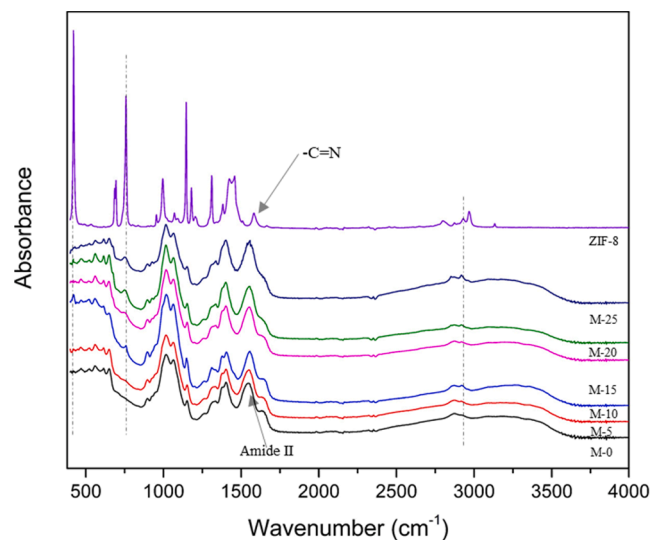


Fig. 5. FTIR spectra of ZIF-8 powders and ZIF-8/CS MMMs with different loadings.

show the characteristic diffraction peak of CS located at $2\theta = 20.2^\circ$ [57]. When compared to the pristine CS membrane, MMMs maintain the same characteristic peak of the pristine CS membrane, showing that the incorporation of ZIF-8 did not influence the crystalline form of CS. Moreover, MMMs show a new peak located around at $2\theta = 34^\circ$, indicating the presence of ZIF-8 within MMMs. The disappearance of some ZIF-8 diffraction peaks in ZIF-8-based MMMs can be attributed to the high affinity between the lattice planes of ZIF-8 and CS polymer backbone [58,59].

3.2.3. FTIR spectroscopy analysis of membranes

The chemical functional groups of the ZIF-8 powder, the pure CS membrane and the MMMs were evaluated using FTIR (Fig. 5). It showed remarkable bands at 426, 694, 760, 955, 1000, 1073, 1146, 1181, 1309, 1385, 1425, 1458, 1585, 1585, 2805, 2929, 2972 and 3135 cm^{-1} for ZIF-8 samples. The peak at 2929 cm^{-1} was ascribed to the aliphatic C-H asymmetric stretching vibration, while peak at 1585 cm^{-1} arose from the C = N stretch vibration. Another peak around 758 cm^{-1} was associated with the bending vibration of the imidazole ring. It is worth noting that Zn-N stretching vibration was observed at 426 cm^{-1} , implying that zinc ions combined chemically with nitrogen atoms of the methylimidazole groups to form the imidazolates [60]. All of that is consistent with the findings from literature [59,61]. The characteristic peaks in the spectrum of ZIF-8 crystals appeared in the FTIR spectrum of

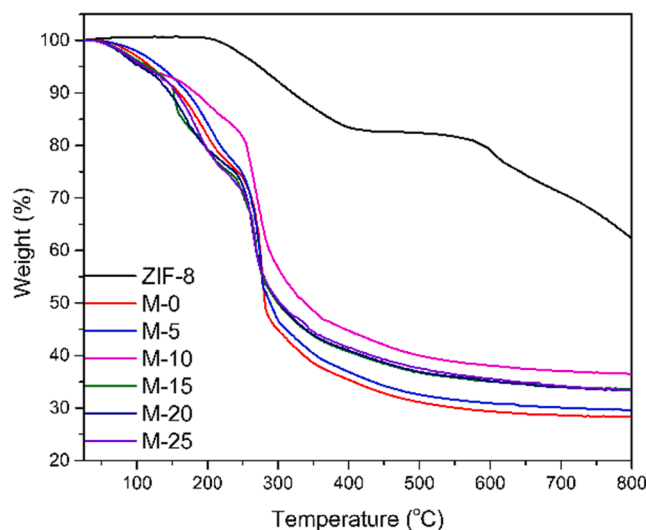


Fig. 6. TGA curves of ZIF-8 powders and ZIF-8/CS MMMs with different loadings.

the MMMs, proving that ZIF-8 particles were successfully incorporated in the CS matrix. Furthermore, no new peaks were found in the spectrum of ZIF-8-based MMMs, showing that there were no chemical interactions formed between ZIF-8 particles and CS polymer. In addition, the peak at around 1550 cm^{-1} for membrane samples representing amide II(N-H) became broad and shifted gradually to the direction of 1585 cm^{-1} , suggesting that N-H groups from CS matrix form intermolecular hydrogen bonds with C = N groups with ZIF-8 [59,62].

3.2.4. TGA analysis of membranes

The thermal stability of ZIF-8 and the membranes with different filler loadings was evaluated by TGA analysis under flowing Ar atmosphere (Fig. 6). The membrane degradation process saw three major weight loss steps. The first step was due to the desorption of the residual water within membranes (below $250\text{ }^{\circ}\text{C}$). The second step was due to the deacetylation and depolymerization of CS ($250\text{--}280\text{ }^{\circ}\text{C}$) and it is the primary step to assess the membrane thermostability. In this step, pristine CS membrane showed a much faster rate of weight loss in comparison with ZIF-8-based MMMs, so the incorporation of ZIF-8 fillers improves membrane thermal stability. This is attributed to the non-chemical interactions (like hydrogen bonds) at the ZIF-8/CS interface, delaying the non-oxidative thermal degradation of ZIF-8 based MMMs and restraining the production of the free radicals during the membrane samples' thermal degradation process. Finally, the third step corresponds to the residual disintegration of the polymer matrix ($280\text{--}800\text{ }^{\circ}\text{C}$). Indeed, ZIF-8-based MMMs possess desirable thermal stability to withstand the experimental operation requirements. Among pure chitosan membrane and MMMs, the highest residual weight achieved is with 10 wt% loading, which is attributed by the uniform dispersion of ZIF-8 particles. The uniformly distributed ZIF-8 particles might form a network through intermolecular hydrogen bonds between chitosan chains and ZIF-8, which restricts the free radicals' movement. And also, the chitosan chain can enter into the pore of residual carbonized ZIF-8 structure during the thermal decomposition process. Above interactions can endow the membrane molecules higher resistance to the attacks from chain scissoring, thus leading to higher residual weight [63]. Such results imply that ZIF-8 does not play a role of simple physical filler in chitosan matrix during the thermal decomposition process, because the incorporation of other inorganic fillers usually promotes more linear increase in the residual weights with the amount of the added filler [64,65].

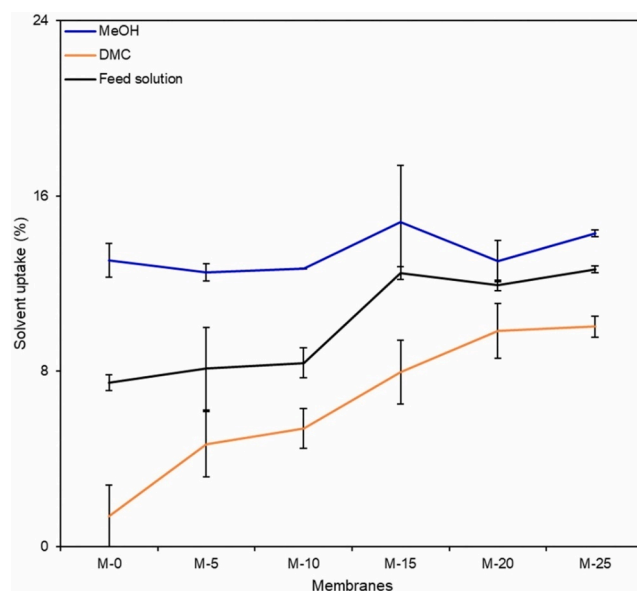


Fig. 7. Solvent uptake of MMMs with different loadings in pure MeOH, DMC and feed solution, respectively.

Table 1

Hansen solubility parameters δ_d , δ_p , δ_h for pure CS [68], ZIF-8 [46], MeOH and DMC [16] and the interaction R_a with CS and ZIF-8.

	$\delta_d(\text{MPa}^{1/2})$	$\delta_p(\text{MPa}^{1/2})$	$\delta_h(\text{MPa}^{1/2})$	$R_a(\text{-CS})$	$R_a(\text{-ZIF-8})$
CS	17.8	14.2	24.1	0	15.0
ZIF-8 ^a	18.8	10.7	9.7	15.0	0
MeOH	15.1	12.3	22.3	6.0	14.7
DMC	15.5	3.9	9.7	18.3	9.5
Feed solution	15.5	4.3	10.3	17.6	9.2

^a Due to the lack of Hansen solubility parameters of ZIF-8, the Hansen solubility parameters of Hmim, the organic ligand in ZIF-8, is taken as the one for interactions with other components.

3.3. Solvent uptake tests of membranes

At $50\text{ }^{\circ}\text{C}$, the solvent uptake of the membranes with different ZIF-8 loadings in DMC and feed solution increased with the increased filler loadings, while the MeOH uptake showed no significant change with the presence of ZIF-8 particles (Fig. 7). Most importantly, the MeOH uptake by the MMMs was higher than the uptake of DMC, showing a preferential sorption to MeOH by CS matrix. Given the solution-diffusion mechanism in pervaporation, preferential sorption of MeOH is of great importance for achieving effective separation [66,67].

Based on the Hansen solubility theory, the smaller the Hansen solubility parameter R_a between two components, the better the compatibility between these two components. As observed in Table 1, the R_a distance between CS and MeOH and DMC are 6.0 and $18.3\text{ MPa}^{1/2}$ respectively, reflecting that the CS membrane have more affinity towards MeOH than DMC. However, the R_a distance between ZIF-8 and MeOH and DMC are 14.7 and $9.5\text{ MPa}^{1/2}$, respectively, which suggests that the ligand of ZIF-8 has a stronger affinity to DMC in comparison with MeOH. Therefore, the major fraction of MeOH is mainly absorbed by the CS matrix while the major fraction of DMC is mainly absorbed by ZIF-8 for MMMs in solvents, considering the flexibility or the "gate opening" effect of the ZIFs [69,70]. Although ZIF-8 ligands show higher affinity to DMC over MeOH, ZIF-8 with suitable aperture size can provide channels across the membranes for MeOH absorbed in the membrane. In the following sections, the influence of ZIF-8 loadings on membrane performance in pervaporation will be discussed

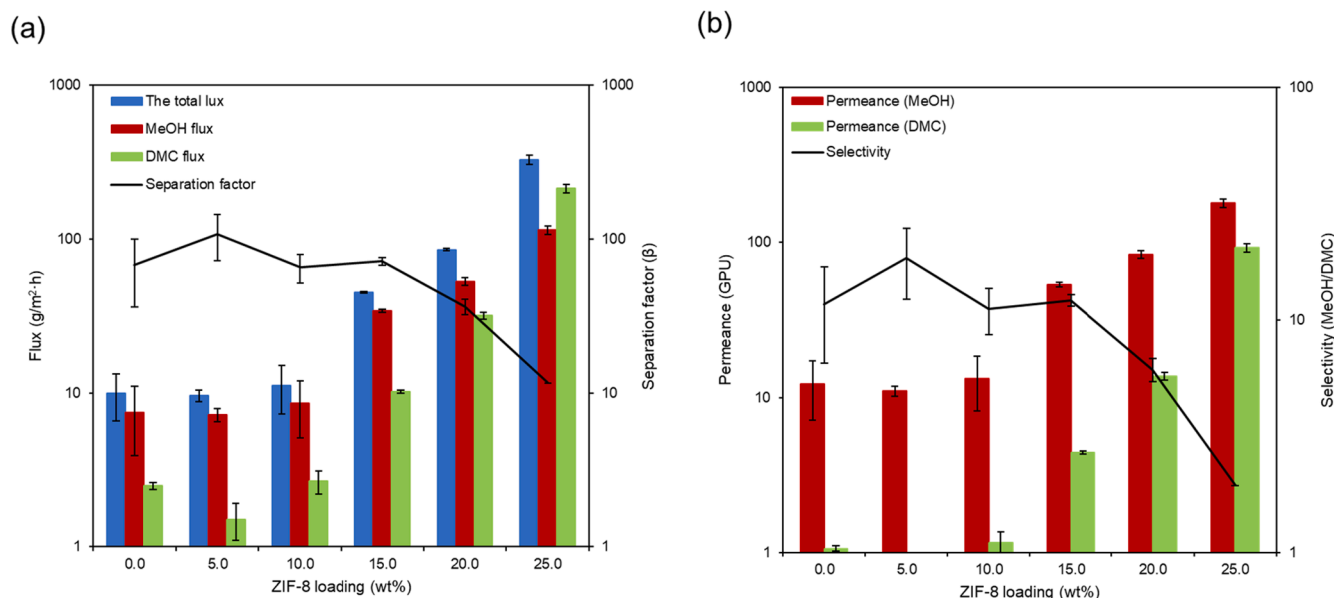


Fig. 8. (a) Effects of ZIF-8 loading on fluxes and separation factor and (b) MeOH permeance, DMC permeance and selectivity as a function of ZIF-8 loading for the separation of MeOH from MeOH/DMC mixture with the mole ratio of 10/90 at 50 °C.

comprehensively.

3.4. Pervaporation performance

3.4.1. Effect of ZIF-8 loading on pervaporation performance

At 50 °C, the permeate flux through the ZIF-8/CS membrane with a loading of 15 wt% and a thickness of ~40 μm increased 4.5 times compared to the pristine CS membrane. Besides, with separation factor increased with 5.9% (Fig. 8a). The MMM with 15 wt% loading of ZIF-8 was identified as the optimum filler loading, in which the separation factor almost remained constant. Beyond this point, even if the permeate flux increases, the separation factor deteriorates.

To further reflect on the inherent separation characteristics of the ZIF-8/CS MMMs, the effect of ZIF-8 incorporation on permeance and selectivity was evaluated. The permeance of MeOH, which was higher than that of DMC, increased with the increment of ZIF-8 content. The optimum MeOH permeance and selectivity was observed at 15 wt% of

ZIF-8 loading, where the selectivity exhibited 3.7% increase, while the MeOH permeance increased more than 4 times compared to the pristine membrane. At this loading, the selectivity was 12.2 and the permeance of MeOH and DMC was 53.4 and 4.4 GPU, respectively. This is ascribed to the factor that ZIF-8 provides preferential diffusion channels for MeOH adsorbed by CS matrix. The molecular kinetic diameter of MeOH (0.38 nm) is smaller than the window size of ZIF-8 (0.40–0.42 nm). However, the ligand of ZIF-8 shows a stronger affinity to DMC though it has a molecular kinetic diameter of 0.47–0.63 nm. The increase of permeance, particularly DMC's, with the increment of the ZIF-8 content was expected due to the enlarged non-selective voids as shown in SEM images (Fig. 2), induced by the distribution of ZIF-8 particles into CS [71]. In the lower loadings (<15 wt%), the aggregation of particles resulted in less enlargement of the non-selective voids, so the increase in MeOH permeance was more apparent than that of DMC. This agglomeration of ZIF-8 particles in the CS matrix becomes more significant with further increase of the filler content that leads to larger non-selective

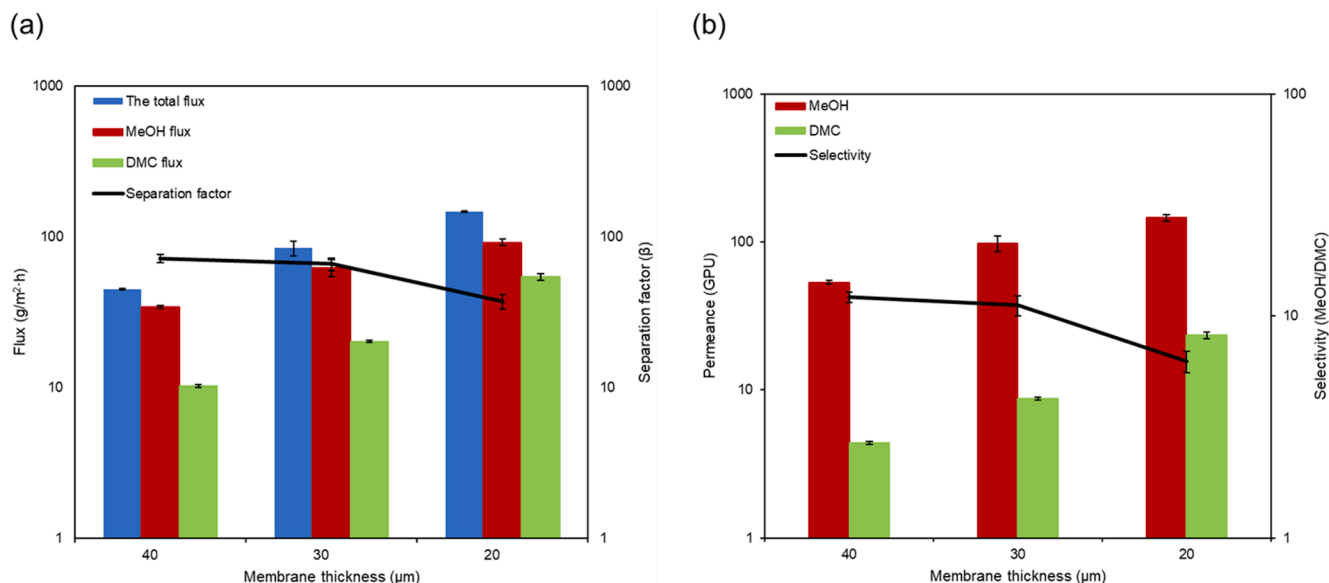


Fig. 9. Effect of membrane thickness on pervaporation performance of ZIF-8/CS MMM: a) fluxes and separation factor; b) permeance and selectivity.

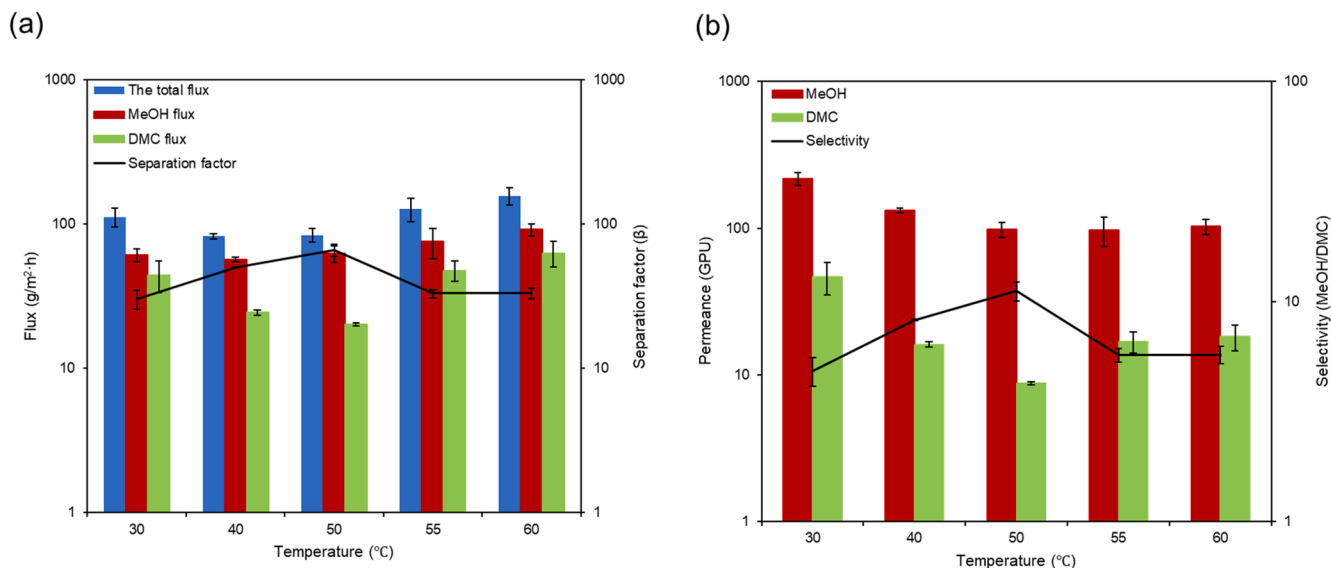


Fig. 10. Effect of feed temperature on pervaporation performance of ZIF-8/CS MMM: a) fluxes and separation factor; b) permeance and selectivity.

voids in the membranes. The higher the ZIF-8 loading the higher the amount of DMC was being absorbed in the MMMs (as depicted in Fig. 7). Therefore, the increase of DMC permeance rate is faster than that of MeOH with a further increase of the filler content at higher loadings than 15 wt%. Considering the MeOH permeance and selectivity, the 15 wt% ZIF-8 loading distributed into CS matrix was selected for the following experiments.

3.4.2. Effect of membrane thickness on pervaporation performance

At 50 °C, starting from the same feed solution concentration (with the MeOH/DMC mole fraction of 10:90), a decrease of the membrane thickness from ~40 to ~20 μm, increased the total flux and the MeOH permeance from 44.96 to 147.4 g/m²·h and from 53.43 to 145.4 GPU respectively. On the other hand, the separation factor and the selectivity decreased from 71.8 to 37.2 and from 12.2 to 6.25 respectively, which is attributed to the greater mass transfer resistance (as shown in Fig. 9a and Fig. 9b). It is worth noting that a more pronounced increase of 82.91% was observed for the MeOH permeance, as the membrane thickness was decreased from ~40 to ~30 μm (Fig. S7), while selectivity only changed by 8.22%. A further decrease of membrane thickness from ~30 to ~20 μm (Fig. S6) caused both the separation factor and the selectivity to drop sharply while the flux and the MeOH permeance increased significantly. With the decrease in membrane thickness, the concentration polarization effect (CPE) could occur [72,73]. That is because that the decrease in membrane thickness provides a higher transmembrane flux, but increases the boundary layer effect between the membrane surface and the feed liquid bulk [74,75]. The increased boundary layer effect, due to the accumulated DMC molecules from the bulk onto the membrane surface, enhances DMC molecules transported across the membrane, thereby reducing MeOH permeance as well as selectivity. Therefore, ~30 μm thick membranes were used for the rest of the study.

3.4.3. Effect of feed solution temperature on pervaporation performance

The effect of the feed temperature on the pervaporation of MeOH/DMC mixture (10/90 mol%) was studied using the membrane with a thickness of ~30 μm and 15 wt% loaded ZIF-8 MMM, as shown in Fig. 10 a and b. As the feed temperature increases, the flux first decreased slightly and then increased, the same trends were observed for MeOH and DMC permeance. This phenomenon can be analyzed by the Arrhenius equation (10):

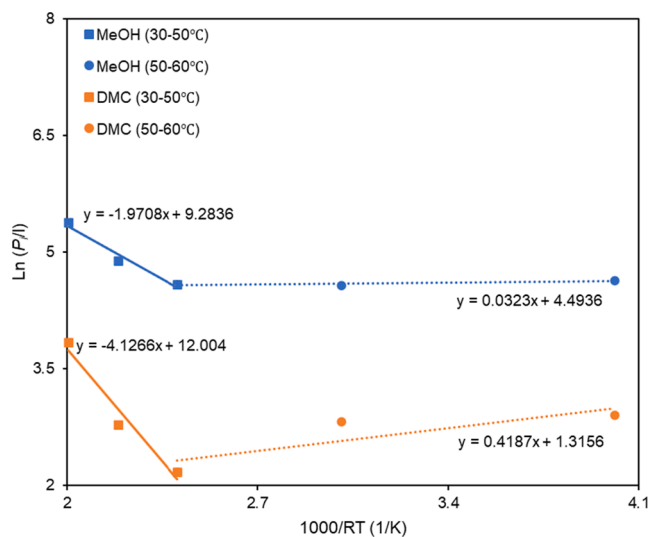


Fig. 11. The Arrhenius plots of permeances versus reciprocal of absolute temperature.

$$P_i/l = P_{i,\infty}/l \cdot \exp\left(-\frac{1000 \cdot E_a}{RT}\right) \quad (10)$$

Wherein P_i/l is the permeance of compound i , $P_{i,\infty}/l$ is the permeance constant, R is the gas constant ($\text{J mol}^{-1} \text{K}^{-1}$), T stands for the feed temperature (K) and E_a represents the activation energy (kJ mol^{-1}).

The Arrhenius plots between MeOH permeance and DMC permeance vs. temperature in the two temperature ranges are shown in Fig. 11. Using a linear fitting to draw the graph logarithmized permeance versus $1000/RT$ according to the equation (10), the calculated activation energies of MeOH and DMC are -0.0323 and -0.419 kJ/mol, respectively. A negative activation energy indicates that MeOH and DMC permeances decrease with the temperature increase, while the flux increases in the temperature range of 40–50 °C. The activation energy of component i is the combination of the activation energy of diffusion $E_{D,i}$ (generally positive) and the enthalpy of sorption $\Delta H_{S,i}$ (usually negative) of component i [76]:

$$E_{a,i} = E_{D,i} + \Delta H_{S,i} \quad (11)$$

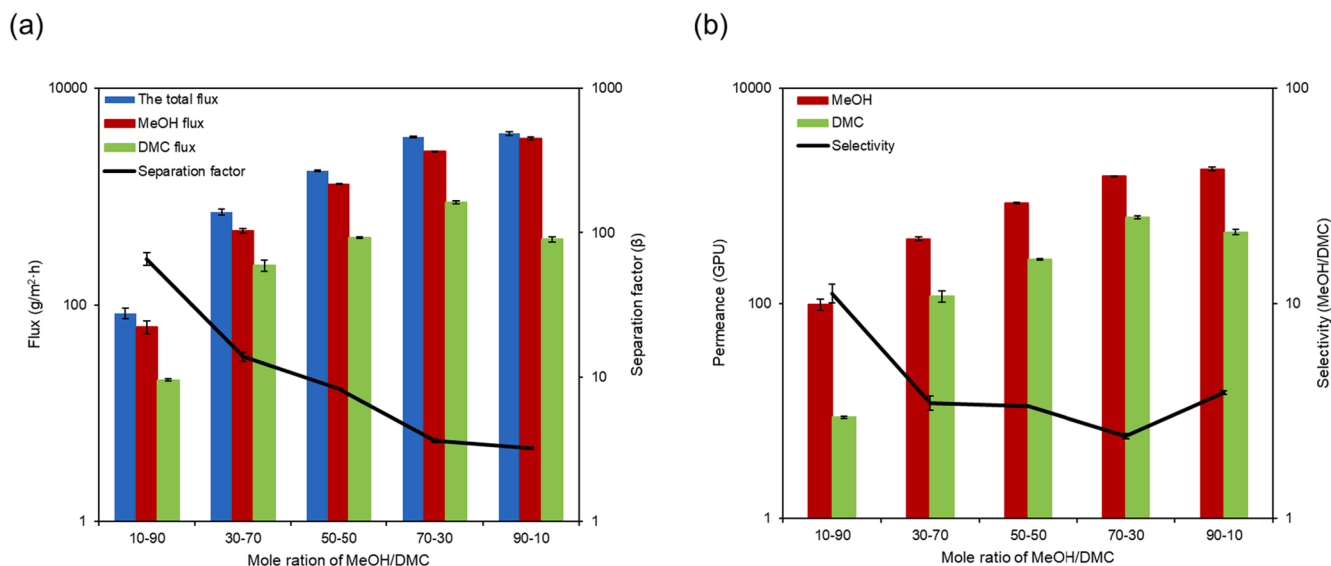


Fig. 12. Effect of the feed concentration on pervaporation performance of ZIF-8/CS MMMs: (a) Fluxes and separation factor; (b) MeOH permeance, DMC permeance and selectivity.

The negative activation energies reflect that in the 15 wt% loaded ZIF-8 MMM, the separation is dominated by the sorption process in the temperature range of 30–50 °C [77]. It means that MeOH and DMC permeances decrease with an increase of the temperature because the sorption process is exothermic, though the polymer chains are prone to swell with a temperature increase, resulting in an increase in the size of non-selective free volumes. The steeper slope of the fitting line for DMC reflects that DMC permeance across the membrane is more sensitive to the temperature. Thus, DMC permeance decreased faster than MeOH permeance as the temperature increased, resulting in an increased selectivity. In addition, the membrane showed a stronger affinity to MeOH over DMC (Table 1), the capacity of MeOH adsorbed in the membrane was higher than that of DMC. Consequently, a higher feed temperature was more favorable to the diffusion transfer of MeOH because of the higher driving force of MeOH, therefore improving the selectivity.

However, the calculated activation energies for MeOH and DMC are 1.97 and 4.13 kJ mol⁻¹, respectively from 50 to 60 °C. These positive values of the activation energies of MeOH and DMC indicate that permeances increase with an increase of temperature. In this temperature range, the separation is controlled by the diffusion process. The polymer swells further with a further increase of temperature, which enlarges the size of non-selective free volumes and thus decreasing the diffusion resistance of molecules. As a result, the permeances of MeOH and DMC increased when the temperature was in the range of 50–60 °C. In addition, the permeance of DMC through the membrane is still more sensitive to temperature because the E_a of DMC is higher than that of the E_a for MeOH. Therefore, the DMC permeance increase more quickly than that of MeOH with the increase of temperature, leading to the increase in selectivity. Nevertheless, the membrane still demonstrated a high selectivity of 11.2 with a separation factor of 66.0 at 50 °C.

3.4.4. Effect of feed concentration on pervaporation performance

The effect of the feed concentration on pervaporation performance was investigated at 50 °C using ~30 μm thick MMMs with 15 wt% ZIF-8 loading. The total flux continuously increased as the mole concentration of MeOH increased (Fig. 12). This increase is mostly influenced by MeOH permeance due to the high MeOH content in the feed solution.

The permeances of MeOH (Fig. 12b) verify the contribution of MeOH to the flux rise. The high MeOH concentration resulted in excessive membrane swelling, and subsequently significant polymer plasticization effect [78]. This results in an enlargement of the size of non-selective

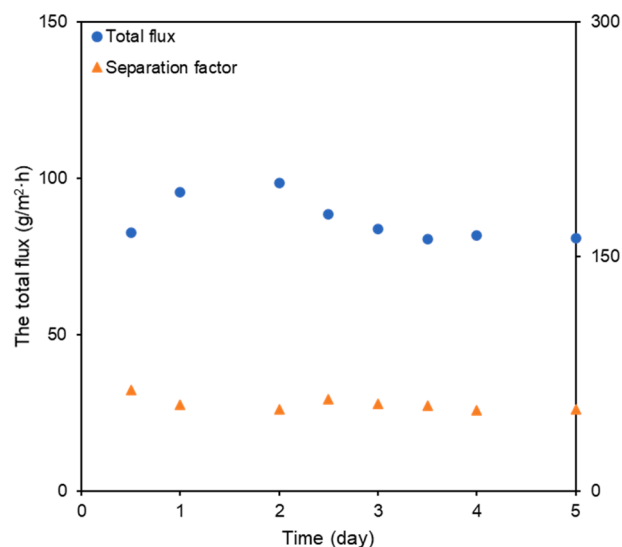


Fig. 13. Long-term PV performance of the 15 wt% ZIF-8/CS MMM (feed temperature: 50 °C, feed composition: the mole ratio of MeOH/DMC of 10/90).

free volumes, which was conducive to the penetration of MeOH and DMC. At low MeOH concentrations, the MeOH permeance increased less quicker than the DMC permeance because the transport of DMC molecules through the membrane was more sensitive to the expansion of the polymer chain spacing because of its larger kinetic diameter [79]. This was also the reason for the decrease of the selectivity at low MeOH concentrations. However, DMC permeance decreased at the highest MeOH concentration because of the lower content of DMC in feed. It can be also explained that at such a concentration, CPE is to enhance the more permeable component (MeOH) permeance while the permeance for the less permeable component (DMC) is slowed down by the boundary layer effect [72]. Therefore, the selectivity increased at the highest MeOH concentration, while separation factor continuously decreased. Notably, the membrane had the highest selectivity of 11.2 at feed concentration MeOH/DMC of 10–90 mol% (3.8 wt% MeOH in feed solution).

Table 2
Comparison of pervaporation performances of methanol/DMC separation membranes in literature.

Membrane	Feed MeOH concentration (mol %)	Feed MeOH concentration (wt %)	Temperature (°C)	The total flux (g/m ² ·h)	MeOH flux (g/m ² ·h)	Separation factor	MeOH permeance (GPU)	Selectivity	Ref.
Chitosan/silica	55	30	50	1158		41.4			[14]
Crosslinked Poly(vinyl alcohol)/poly(acrylic acid)	86.8	70	70	248		37			[83]
SiO ₂ -ZrO ₂	53	29	50	100	96.12	10	66.4	4.2	[84]
Polyamide-6/ZrO ₂	41.3	20	30	199		6			[85]
Silicotungstic acid hydrate/Chitosan	23.8	10	50	1163		67.3			[86]
Chitosan hollow fiber membrane	86.8	70	50	~ 430		~ 5.3			[87]
Chitosan crosslinked with H ₂ SO ₄	53.5	29	25	~ 81		~ 38			[88]
Chitosan	12.9	5	45	~ 40	~ 25	~ 53			[89]
Chitosan crosslinked with APTEOS	74	50	50	1225		39.4			[14]
Poly(vinyl alcohol)/poly(acrylic acid)	86.8	70	60	~ 577	~ 540	~ 13			[90]
Poly ether ether ketone modified with cardo group	10	3.8	30	140		13.4	293	3.5	[16]
40 μm Chitosan/ZIF-8	10	3.8	50	45.0	34.3	71.8	53.4	12.2	This study
30 μm Chitosan/ZIF-8	10	3.8	30	112.0	61.3	30.2	217.1	4.8	This study
30 μm Chitosan/ZIF-8	10	3.8	40	82.3	57.1	50.1	132.5	8.2	This study
30 μm Chitosan/ZIF-8	10	3.8	50	84.2	62.5	66.0	97.7	11.2	This study
30 μm Chitosan/ZIF-8	10	3.8	60	156.4	91.8	33.2	102.5	5.7	This study

3.5. Long-term durability of the ZIF-8/ CS MMMs

The stability of the ~ 30 μm thick MMM with the 15 wt% ZIF-8 loading was monitored for 5 consecutive days, as depicted in Fig. 13. It demonstrates that the total flux and separation factor fluctuated slightly with the operating time. In summary, both the total flux and separation factor maintained relatively stable during the 5-day measurement.

3.6. Comparison with literature data

Table 2 shows the literature comparison of the MeOH/DMC pervaporation separation performance of different membranes. In this work, it is shown that ZIF-8/CS membranes exhibit a superb performance under low MeOH concentration (10/90 mol%) with 97.7 GPU MeOH permeance and 11.2 selectivity at 50 °C. This superior performance is better than any other pre-existing membranes tested under similar conditions. This work opens new opportunities for purifying DMC when a small quantity of MeOH exists in the mixture. This separation not only helps with the synthesis of DMC using MeOH but also in the transesterification of glycerol and DMC [80,81]. In the latter example, the transesterification process can be combined with the reaction and pervaporation [82], in which the small amount of methanol as a side product in the mixture is removed using membrane pervaporation, thereby shifting the equilibrium to the right.

4. Conclusions

This study showcased a breakthrough in the azeotrope limitation in the separation of binary organic mixtures. A MeOH/DMC mixture mole fraction was flipped from 10:90 to ~ 90:10 with pervaporation, thanks to the developed mixed matrix membranes comprising a chitosan self-standing membrane with incorporated ZIF-8 fillers. The CS matrix showed higher affinity towards MeOH, which was further reinforced

with the preferential channel of the embedded ZIF-8 particles. The optimized ZIF-8 loading of 15 wt% was identified, where the MeOH permeance increased without hindering selectivity, in comparison with pure CS membrane. A permeance-selectivity trade-off was monitored when changing the membrane thickness and MeOH feed concentration. The temperature effect showed that the separation was dominated by the sorption mechanism under low temperature, while the diffusion mechanism dominated the separation process under high temperature condition. Finally, the optimum MMM with the thickness of ~ 30 μm exhibited the total flux of 84.2 g/m²·h (MeOH permeance of 97.7 GPU) and a separation factor of 66.0 (selectivity of 11.2) at low MeOH concentration (0.1 M fraction).

CRediT authorship contribution statement

Xiao Xu: Conceptualization, Methodology, Validation, Formal analysis, Investigation, Writing – original draft, Writing – review & editing, Visualization. **Yusak Hartanto:** Conceptualization, Writing – review & editing. **Daria Nikolaeva:** Conceptualization, Methodology. **Zirui He:** Investigation. **Sara Chergaoui:** Writing – review & editing. **Patricia Luis:** Writing – review & editing, Supervision.

Declaration of Competing Interest

The authors declare that they have no known competing financial interests or personal relationships that could have appeared to influence the work reported in this paper.

Acknowledgments

Xiao Xu acknowledges the funding from the China Scholarship Council (CSC, No.201906050060). The authors would like to thank Professor Juray De Wilde, and Professor Damien P. Debecker for access to the TGA and FTIR equipment respectively. We also thank François

Devred for conducting the FTIR tests.

Appendix A. Supplementary material

Supplementary data to this article can be found online at <https://doi.org/10.1016/j.seppur.2022.121085>.

References

- P. Tundo, et al., Dimethyl Carbonate: Green Solvent and Ambident Reagent, Dordrecht, Springer Netherlands, 2008.
- J. Yang, Y.u. Jiang, G. Karavalakis, K.C. Johnson, S. Kumar, D.R. Cocker, T. D. Durbin, Impacts of dimethyl carbonate blends on gaseous and particulate emissions from a heavy-duty diesel engine, *Fuel* 184 (2016) 681–688.
- P. Sharan, et al., Effect of dimethyl carbonate on performance and emission characteristics of a diesel engine, *Int. J. Curr. Res. Rev* 10 (2018) 116–121.
- P. Rounce, A. Tsolakis, P. Leung, A.P.E. York, A comparison of diesel and biodiesel emissions using dimethyl carbonate as an oxygenated additive, *Energy Fuels* 24 (9) (2010) 4812–4819.
- M. Pan, et al., Effects of dimethyl carbonate and 2-ethylhexyl nitrate on energy distribution, combustion and emissions in a diesel engine under different load conditions, *Energy Convers. Manage.* 199 (2019), 111985.
- D. Mei, K. Hielscher, R. Baar, Study on combustion process and emissions of a single-cylinder diesel engine fueled with DMC/diesel blend, *J. Energy Eng.* 140 (1) (2014) 04013004, [https://doi.org/10.1061/\(ASCE\)EY.1943-7897.0000168](https://doi.org/10.1061/(ASCE)EY.1943-7897.0000168).
- L. Aguado-Deblas, J. Hidalgo-Carrillo, F.M. Bautista, C. Luna, J. Calero, A. Posadillo, A.A. Romero, D. Luna, R. Estévez, Evaluation of dimethyl carbonate as alternative biofuel. performance and smoke emissions of a diesel engine fueled with diesel/dimethyl carbonate/straight vegetable oil triple blends, *Sustainability* 13 (4) (2021) 1749, <https://doi.org/10.3390/su13041749>.
- Y. Ono, Dimethyl carbonate for environmentally benign reactions, *Catal. Today* 35 (1–2) (1997) 15–25.
- X. Yang, H.S. Choi, J.H. Lee, S.K. Lee, S.O. Han, C. Park, S.W. Kim, Improved production of 1, 3-propanediol from biodiesel-derived crude glycerol by *Klebsiella pneumoniae* in fed-batch fermentation, *Chem. Eng. J.* 349 (2018) 25–36.
- P. Juszczak, L. Tomaszewska, A. Kita, W. Rymowicz, Biomass production by novel strains of *Yarrowia lipolytica* using raw glycerol, derived from biodiesel production, *Bioresour. Technol.* 137 (2013) 124–131.
- W.K. Teng, G.C. Ngoh, R. Yusoff, M.K. Aroua, Microwave-assisted transesterification of industrial grade crude glycerol for the production of glycerol carbonate, *Chem. Eng. J.* 284 (2016) 469–477.
- P. Lu, H. Wang, K. Hu, Synthesis of glycerol carbonate from glycerol and dimethyl carbonate over the extruded CaO-based catalyst, *Chem. Eng. J.* 228 (2013) 147–154.
- P. Devi, U. Das, A.K. Dalai, Production of glycerol carbonate using a novel Ti-SBA-15 catalyst, *Chem. Eng. J.* 346 (2018) 477–488.
- J.H. Chen, Q.L. Liu, J. Fang, A.M. Zhu, Q.G. Zhang, Composite hybrid membrane of chitosan-silica in pervaporation separation of MeOH/DMC mixtures, *J. Colloid Interface Sci.* 316 (2) (2007) 580–588.
- W.-Z. Liu, D.-H. Wong, S.-J. Wang, H.-C. Hsu, Effect of mass transfer on the design of an extractive distillation process for separating DMC and methanol, *J. Taiwan Inst. Chem. Eng.* 60 (2016) 205–212.
- W. Li, F. Galiano, J. Estager, J.-C. Monbaliu, D.P. Debecker, A. Figoli, P. Luis, Sorption and pervaporation study of methanol/dimethyl carbonate mixture with poly (etheretherketone)(PEEK-WC) membrane, *J. Membr. Sci.* 567 (2018) 303–310.
- Z. Zhang, et al., Separation of methanol+ dimethyl carbonate azeotropic mixture using ionic liquids as entrainers, *Fluid Phase Equilib.* 435 (2017) 98–103.
- D.P. Suhas, T.M. Aminabhavi, A.V. Raghunath, Mixed matrix membranes of H-ZSM5-loaded poly (vinyl alcohol) used in pervaporation dehydration of alcohols: influence of silica/alumina ratio, *Polym. Eng. Sci.* 54 (8) (2014) 1774–1782.
- B. Smitha, et al., Separation of organic-organic mixtures by pervaporation—a review, *J. Membr. Sci.* 241 (1) (2004) 1–21.
- S. Fazlifard, T. Mohammadi, O. Bakhtiari, Chitosan/ZIF-8 mixed-matrix membranes for pervaporation dehydration of isopropanol, *Chem. Eng. Technol.* 40 (4) (2017) 648–655.
- M.S. Jyothi, K.R. Reddy, K. Soontarapa, S. Naveen, A.V. Raghunath, R.V. Kulkarni, D. P. Suhas, N.P. Shetti, M.N. Nadagouda, T.M. Aminabhavi, Membranes for pervaporation of alcohols via pervaporation, *J. Environ. Manage.* 242 (2019) 415–429.
- X. Xu, D. Nikolaeva, Y. Hartanto, P. Luis, MOF-based membranes for pervaporation, *Sep. Purif. Technol.* 278 (2021) 119233, <https://doi.org/10.1016/j.seppur.2021.119233>.
- X.H. Zhang, Q.L. Liu, Y. Xiong, A.M. Zhu, Y.u. Chen, Q.G. Zhang, Pervaporation dehydration of ethyl acetate/ethanol/water azeotrope using chitosan/poly (vinyl pyrrolidone) blend membranes, *J. Membr. Sci.* 327 (1–2) (2009) 274–280.
- V.T. Magalad, G.S. Gokavi, M.N. Nadagouda, T.M. Aminabhavi, Pervaporation separation of water-ethanol mixtures using organic-inorganic nanocomposite membranes, *J. Phys. Chem. C* 115 (30) (2011) 14731–14744.
- F. Peng, et al., Hybrid organic-inorganic membrane: solving the tradeoff between permeability and selectivity, *Chem. Mater.* 17 (26) (2005) 6790–6796.
- K.M. Gheimasi, M. Peydayesh, T. Mohammadi, O. Bakhtiari, Prediction of CO₂/CH₄ permeability through Sigma-1–Matrimid® 5218 MMMs using the Maxwell model, *J. Membr. Sci.* 466 (2014) 265–273.
- K. Mohammad Gheimasi, T. Mohammadi, O. Bakhtiari, Modification of ideal MMMs permeation prediction models: effects of partial pore blockage and polymer chain rigidification, *J. Membr. Sci.* 427 (2013) 399–410.
- R. Pal, New models for thermal conductivity of particulate composites, *J. Reinf. Plast. Compos.* 26 (7) (2007) 643–651.
- Shu, S. Husain, W.J. Koros, A general strategy for adhesion enhancement in polymeric composites by formation of nanostructured particle surfaces, *J. Phys. Chem. C* 111 (2) (2007) 652–657.
- J. Ahn, W.-J. Chung, I. Pinnau, M.D. Guiver, Polysulfone/silica nanoparticle mixed-matrix membranes for gas separation, *J. Membr. Sci.* 314 (1–2) (2008) 123–133.
- B. Zornoza, B. Seoane, J.M. Zamoro, C. Téllez, J. Coronas, Combination of MOFs and zeolites for mixed-matrix membranes, *ChemPhysChem* 12 (15) (2011) 2781–2785.
- B. Zornoza, C. Téllez, J. Coronas, J. Gascon, F. Kaptejin, Metal organic framework based mixed matrix membranes: an increasingly important field of research with a large application potential, *Micropor. Mesopor. Mater.* 166 (2013) 67–78.
- F. Ahmadijokani, et al., Superior chemical stability of UiO-66 metal-organic frameworks (MOFs) for selective dye adsorption, *Chem. Eng. J.* 399 (2020), 125346.
- K.S. Park, Z. Ni, A.P. Côté, J.Y. Choi, R. Huang, F.J. Uribe-Romo, H.K. Chae, M. O’Keeffe, O.M. Yaghi, Exceptional chemical and thermal stability of zeolitic imidazolate frameworks, *Proc. Natl. Acad. Sci.* 103 (27) (2006) 10186–10191.
- M. Amirilargani, B. Sadatnia, Poly (vinyl alcohol)/zeolitic imidazolate frameworks (ZIF-8) mixed matrix membranes for pervaporation dehydration of isopropanol, *J. Membr. Sci.* 469 (2014) 1–10.
- D. Hua, Y.K. Ong, Y. Wang, T. Yang, T.-S. Chung, ZIF-90/P84 mixed matrix membranes for pervaporation dehydration of isopropanol, *J. Membr. Sci.* 453 (2014) 155–167.
- S. Liu, G. Liu, X. Zhao, W. Jin, Hydrophobic-ZIF-71 filled PEBA mixed matrix membranes for recovery of biobutanol via pervaporation, *J. Membr. Sci.* 446 (2013) 181–188.
- C.-H. Kang, Y.-F. Lin, Y.-S. Huang, K.-L. Tung, K.-S. Chang, J.-T. Chen, W.-S. Hung, K.-R. Lee, J.-Y. Lai, Synthesis of ZIF-7/chitosan mixed-matrix membranes with improved separation performance of water/ethanol mixtures, *J. Membr. Sci.* 438 (2013) 105–111.
- T. Wu, J. Lucero, M.A. Sinnwell, P.K. Thallapally, M.A. Carreon, Recovery of xenon from air over ZIF-8 membranes, *Chem. Commun.* 54 (65) (2018) 8976–8979.
- C. Zhang, R.P. Lively, K.e. Zhang, J.R. Johnson, O. Karvan, W.J. Koros, Unexpected molecular sieving properties of zeolitic imidazolate framework-8, *J. Phys. Chem. Lett.* 3 (16) (2012) 2130–2134.
- Z. Shariatnia, M. Fazli, Mechanical properties and antibacterial activities of novel nanobiocomposite films of chitosan and starch, *Food Hydrocolloids* 46 (2015) 112–124.
- N.A.H.M. Nordin, A.F. Ismail, A. Mustafa, P.S. Goh, D. Rana, T. Matsuura, Aqueous room temperature synthesis of zeolitic imidazole framework 8 (ZIF-8) with various concentrations of triethylamine, *RSC Adv.* 4 (63) (2014) 33292–33300.
- K. Leus, T. Bogaerts, J. De Decker, H. Depauw, K. Hendrickx, H. Vrielandck, V. Van Speybroeck, P. Van Der Voort, Systematic study of the chemical and hydrothermal stability of selected “stable”, *Met. Org. Frameworks Micropor. Mesopor. Mater.* 226 (2016) 110–116.
- Y. Devrim, S. Erkan, N. Baç, I. Eroğlu, Preparation and characterization of sulfonated polysulfone/titanium dioxide composite membranes for proton exchange membrane fuel cells, *Int. J. Hydrogen Energy* 34 (8) (2009) 3467–3475.
- I.G. Veiga, A.M. Moraes, Study of the swelling and stability properties of chitosan-xanthan membranes, *J. Appl. Polym. Sci.* 124 (S1) (2012) E154–E160.
- L. Paseta, G. Potier, S. Abbott, J. Coronas, Using Hansen solubility parameters to study the encapsulation of caffeine in MOFs, *Org. Biomol. Chem.* 13 (6) (2015) 1724–1731.
- C. Casado-Coterillo, A. Fernández-Barquín, B. Zornoza, C. Téllez, J. Coronas, Á. Irabien, Synthesis and characterisation of MOF/ionic liquid/chitosan mixed matrix membranes for CO₂/N₂ separation, *RSC Adv.* 5 (124) (2015) 102350–102361.
- A.F.M. Barton, Solubility parameters, *Chem. Rev.* 75 (6) (1975) 731–753.
- W. Li, et al., Supported ionic liquid membranes for the separation of methanol/dimethyl carbonate mixtures by pervaporation, *J. Membr. Sci.* 598 (2020), 117790.
- W. Li, P. Luis, Understanding coupling effects in pervaporation of multi-component mixtures, *Sep. Purif. Technol.* 197 (2018) 95–106.
- P. Luis, B. Van der Bruggen, The driving force as key element to evaluate the pervaporation performance of multicomponent mixtures, *Sep. Purif. Technol.* 148 (2015) 94–102.
- S. Yu, Z. Jiang, H.e. Ding, F. Pan, B. Wang, J. Yang, X. Cao, Elevated pervaporation performance of polysiloxane membrane using channels and active sites of metal organic framework CuBTC, *J. Membr. Sci.* 481 (2015) 73–81.
- Y. Pan, Y. Liu, G. Zeng, L. Zhao, Z. Lai, Rapid synthesis of zeolitic imidazolate framework-8 (ZIF-8) nanocrystals in an aqueous system, *Chem. Commun.* 47 (7) (2011) 2071, <https://doi.org/10.1039/c0cc05002d>.
- F. Alisafaei, C.-S. Han, Indentation depth dependent mechanical behavior in polymers, *Adv. Condens. Matter Phys.* 2015 (2015) 1–20.
- C.M. Chan, G.Z. Cao, H. Fong, M. Sarikaya, T. Robinson, L. Nelson, Nanoindentation and adhesion of sol-gel-derived hard coatings on polyester, *J. Mater. Res.* 15 (1) (2000) 148–154.

- [56] A. Jamil, M. Zulfiqar, U. Arshad, S. Mahmood, T. Iqbal, S. Rafiq, M.Z. Iqbal, L. Baldino, Development and performance evaluation of cellulose acetate-bentonite mixed matrix membranes for CO₂ separation, *Adv. Polym. Tech.* 2020 (2020) 1–12.
- [57] S. Yang, Y. Wang, H. Li, Y. Zhan, X. Ding, M. Wang, X. Wang, L. Xiao, Synthesis of nano-ZIF-8@ chitosan microspheres and its rapid removal of p-hydroxybenzoic acid from the agro-industry and preservatives, *J. Porous Mater.* 28 (1) (2021) 29–38.
- [58] M. Khajavian, E. Salehi, V. Vatanpour, Nanofiltration of dye solution using chitosan/poly (vinyl alcohol)/ZIF-8 thin film composite adsorptive membranes with PVDF membrane beneath as support, *Carbohydr. Polym.* 247 (2020), 116693.
- [59] Y. Zhang, Y. Jia, Li'an Hou, Synthesis of zeolitic imidazolate framework-8 on polyester fiber for PM 2.5 removal, *RSC Adv.* 8 (55) (2018) 31471–31477.
- [60] Y. Hu, H. Kazemian, S. Rohani, Y. Huang, Y. Song, In situ high pressure study of ZIF-8 by FTIR spectroscopy, *Chem. Commun.* 47 (47) (2011) 12694, <https://doi.org/10.1039/c1cc15525c>.
- [61] Y. Rao, et al., Efficient recovery of the volatile aroma components from blackberry juice using a ZIF-8/PDMS hybrid membrane, *Sep. Purif. Technol.* 230 (2020), 115844.
- [62] J. Chen, J. Guo, M. Zhao, R. Zhang, F. Guan, Hydrogen bonding in chitosan/ Antarctic krill protein composite system: Study on construction and enhancement mechanism, *Int. J. Biol. Macromol.* 142 (2020) 513–520.
- [63] H. Wang, P. Xu, S. Meng, W. Zhong, W. Du, Q. Du, Poly (methyl methacrylate)/ silica/titania ternary nanocomposites with greatly improved thermal and ultraviolet-shielding properties, *Polym. Degrad. Stab.* 91 (7) (2006) 1455–1461.
- [64] K. Chrissafis, K.M. Paraskevopoulos, G.Z. Papageorgiou, D.N. Bikiaris, Thermal and dynamic mechanical behavior of bionanocomposites: fumed silica nanoparticles dispersed in poly (vinyl pyrrolidone), chitosan, and poly (vinyl alcohol), *J. Appl. Polym. Sci.* 110 (3) (2008) 1739–1749.
- [65] L. Cano, E. Pollet, L. Avérus, A. Tercjak, Effect of TiO₂ nanoparticles on the properties of thermoplastic chitosan-based nano-biocomposites obtained by mechanical kneading, *Compos. A Appl. Sci. Manuf.* 93 (2017) 33–40.
- [66] V.S. Cunha, M.L.L. Paredes, C.P. Borges, A.C. Habert, R. Nobrega, Removal of aromatics from multicomponent organic mixtures by pervaporation using polyurethane membranes: experimental and modeling, *J. Membr. Sci.* 206 (1–2) (2002) 277–290.
- [67] X. Wang, J. Chen, M. Fang, T. Wang, L. Yu, J. Li, ZIF-7/PDMS mixed matrix membranes for pervaporation recovery of butanol from aqueous solution, *Sep. Purif. Technol.* 163 (2016) 39–47.
- [68] Y.Z. Zhu Ryberg, U. Edlund, A.-C. Albertsson, Conceptual approach to renewable barrier film design based on wood hydrolysate, *Biomacromolecules* 12 (4) (2011) 1355–1362.
- [69] D. Fairen-Jimenez, S.A. Moggach, M.T. Wharmby, P.A. Wright, S. Parsons, T. Düren, Opening the gate: framework flexibility in ZIF-8 explored by experiments and simulations, *J. Am. Chem. Soc.* 133 (23) (2011) 8900–8902.
- [70] E. Haldoupis, T. Watanabe, S. Nair, D.S. Sholl, Quantifying large effects of framework flexibility on diffusion in MOFs: CH₄ and CO₂ in ZIF-8, *ChemPhysChem* 13 (15) (2012) 3449–3452.
- [71] S.J. Lue, I.-M. Su, D.-T. Lee, H.-Y. Chen, C.-M. Shih, C.-C. Hu, Y.C. Jean, J.-Y. Lai, Correlation between free-volume properties and pervaporative flux of polyurethane– zeolite composites on organic solvent mixtures, *J. Phys. Chem. B* 115 (12) (2011) 2947–2958.
- [72] X. Feng, R.Y.M. Huang, Concentration polarization in pervaporation separation processes, *J. Membr. Sci.* 92 (3) (1994) 201–208.
- [73] I.L. Borisov, A. Kujawska, K. Knozowska, V.V. Volkov, W. Kujawski, Influence of feed flow rate, temperature and feed concentration on concentration polarization effects during separation of water-methyl acetate solutions with high permeable hydrophobic pervaporation PDMS membrane, *J. Membr. Sci.* 564 (2018) 1–9.
- [74] H. Wang, et al., Mass transport and pervaporation recovery of aniline with high-purity from dilute aqueous solution by PEBA/PVDF composite membranes, *Sep. Purif. Technol.* 268 (2021), 118708.
- [75] R. Khan, et al., Enhancing the pervaporation performance of PEBA/PVDF membrane by incorporating MAF-6 for the separation of phenol from its aqueous solution, *Sep. Purif. Technol.* 256 (2021), 117804.
- [76] P. Luis, *Fundamental Modeling of Membrane Systems: Membrane and Process Performance*, Elsevier, 2018.
- [77] P. Luis, J. Degève, B.V. der Bruggen, Separation of methanol–n-butyl acetate mixtures by pervaporation: potential of 10 commercial membranes, *J. Membr. Sci.* 429 (2013) 1–12.
- [78] L. Wenqi, Pervaporation for the separation of transesterification reaction mixtures. 2019, Thèse de doct. université Catholique de Louvain.
- [79] G. Liu, Z. Jiang, K. Cao, S. Nair, X. Cheng, J. Zhao, H. Goma, H. Wu, F. Pan, Pervaporation performance comparison of hybrid membranes filled with two-dimensional ZIF-L nanosheets and zero-dimensional ZIF-8 nanoparticles, *J. Membr. Sci.* 523 (2017) 185–196.
- [80] D. Delle Donne, F. Rivetti, U. Romano, Developments in the production and application of dimethylcarbonate, *Appl. Catal. A* 221 (1–2) (2001) 241–251.
- [81] S. Ramesh, D.P. Debecker, Room temperature synthesis of glycerol carbonate catalyzed by spray dried sodium aluminate microspheres, *Catal. Commun.* 97 (2017) 102–105.
- [82] G.R. Harvianto, F. Ahmad, M. Lee, A hybrid reactive distillation process with high selectivity pervaporation for butyl acetate production via transesterification, *J. Membr. Sci.* 543 (2017) 49–57.
- [83] L. Wang, J. Li, Y. Lin, C. Chen, Crosslinked poly (vinyl alcohol) membranes for separation of dimethyl carbonate/methanol mixtures by pervaporation, *Chem. Eng. J.* 146 (1) (2009) 71–78.
- [84] T. Tsuru, A. Sasaki, M. Kanezashi, T. Yoshioka, Pervaporation of methanol/dimethyl carbonate using SiO₂ membranes with nano-tuned pore sizes and surface chemistry, *AIChE J.* 57 (8) (2011) 2079–2089.
- [85] R. Kopeć, M. Meller, W. Kujawski, J. Kujawa, Polyamide-6 based pervaporation membranes for organic–organic separation, *Sep. Purif. Technol.* 110 (2013) 63–73.
- [86] J.H. Chen, Q.L. Liu, A.M. Zhu, Q.G. Zhang, J. Fang, Pervaporation separation of MeOH/DMC mixtures using STA/CS hybrid membranes, *J. Membr. Sci.* 315 (1–2) (2008) 74–81.
- [87] T. Xiao, X. Xu, Y. Cao, M. Deng, S. Chen, X. Jie, Preparation of asymmetric chitosan hollow fiber membrane and its pervaporation performance for dimethyl carbonate/methanol mixtures, *J. Appl. Polym. Sci.* 115 (5) (2010) 2875–2882.
- [88] W. Won, X. Feng, D. Lawless, Separation of dimethyl carbonate/methanol/water mixtures by pervaporation using crosslinked chitosan membranes, *Sep. Purif. Technol.* 31 (2) (2003) 129–140.
- [89] W. Won, X. Feng, D. Lawless, Pervaporation with chitosan membranes: separation of dimethyl carbonate/methanol/water mixtures, *J. Membr. Sci.* 209 (2) (2002) 493–508.
- [90] L. Wang, J. Li, Y. Lin, C. Chen, Separation of dimethyl carbonate/methanol mixtures by pervaporation with poly (acrylic acid)/poly (vinyl alcohol) blend membranes, *J. Membr. Sci.* 305 (1–2) (2007) 238–246.